ACS OMEGA

http://pubs.acs.org/journal/acsodf

Article

Nickel Coated Polyester Sponge for Delaying the Specific Aggregation of Fine Particles Induced by Negative Air Ions

Chaoying Zhang, Zengnan Wu, Haifeng Lin, Zenghe Li,* and Jin-Ming Lin*

Cite This: *ACS Omega* 2022, 7, 11285−11292

Read Online

ACCESS | Metrics & More | Article Recommendations | Supporting Information

ABSTRACT: Negative air ions (NAIs) produced by corona discharge is often used for indoor air purification; however, the specific aggregation of suspended particles caused by NAIs, especially fine particles (FPs), needs to be considered. Here, a nickel coated conductive sponge (NCCS) was used as the main adsorption interface for delaying the obstinate aggregation caused by NAIs on another surface. The specific aggregation of FPs is caused by the directional transfer of electric charge, and the oxidation characteristic of NAIs results in the surface reaction of FPs simultaneously. The conductivity and roughness of the adsorption interface determine the migration direction and enrichment number of FPs, respectively. Nickel coated conductive sponge with high conductivity and high specific surface area can effectively adsorb the FPs affected by NAIs and can effectively delay the specific aggregation on the surface of indoor objects.

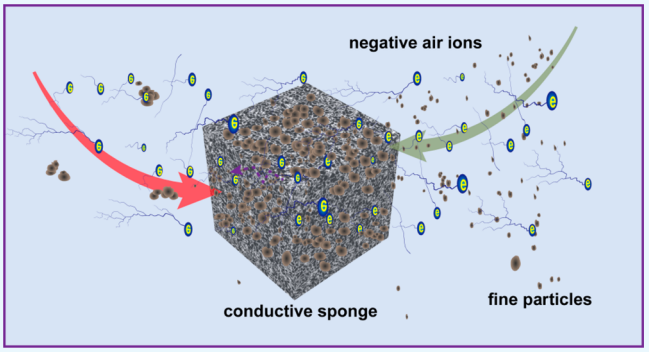

INTRODUCTION

Indoor air quality, especially the concentration of fine particulate matter, is associated with the increased risk of some respiratory diseases.[1−4] The suspended particles are composed of volatile organic compounds (VOCs), heavy metals, silicate, black carbon, and nitrate, which can cause serious health problems, such as asthma, lung cancer, and even mortality.[5−8] Since people spend the majority of their time indoors, scientifically controlling particulate exposure can help eliminate the potential safety risks associated with the particulate matter in an indoor environment.[9] In recent years, many successful approaches have been developed to purify indoor air.[10−12] Physical filtration is one of the typical methods, and the purification efficiency depends on the performance of the filtration materials, such as glass fiber, polyester fiber, and needle-punched fiber.[13,14] However, it is difficult to widely apply these advanced purification materials in residential spaces due to the limitations of lifetime and maintenance cost. Another commonly used air purification technology, electrostatic precipitator (ESP), has been extensively used for cleaning the air in buildings and has a high purification efficiency for fine particles.[15] Negative air ions (NAIs) produced by the corona discharge are a familiar form of ESP, which is widely equipped in various types of household electrical appliances.[16,17] Although NAIs have the advantages of high purification and low production cost, attention should be given to the specific aggregation of particulate matter caused by NAIs.[18]

Specific aggregated particles (SAPs) caused by NAIs are a typical pollutant, which often occur around household appliances and have strong chemical and physical stability. There are few studies on SAPs, so there is no effective way to completely remove or reduce the aggregated particles (APs) on indoor surfaces. These obstinate aggregated particles will continuously release VOCs under heat or sunlight conditions, resulting in persistent damage to human health.[19] Hence, the identification of the mainly compositions in SAPs and the exploration of the conditions affecting particle aggregation are important factors in understanding the formation of SAPs. However, there is relatively little information on the formation progress of SAPs.

The goal of this work is twofold: first, to reveal the truth of SAPs caused by NAIs, including the aggregation process, main compositions, and influencing factors; second, to explore measures to reduce or delay the formation of SAPs. Based on the above goals, we simulated the formation of SAPs in the laboratory. Notably, the experimental environment is almost identical to the daily environment in which the suspended particles are aggregated to form SAPs. We fixed different materials on the wall to replace the adsorption surface to collect APs. The concentration of NAIs was artificially increased to accelerate the aggregation of particles. All the

Received: January 14, 2022
Accepted: March 11, 2022
Published: March 24, 2022

https://doi.org/10.1021/acsomega.2c00290
ACS Omega 2022, 7, 11285−11292

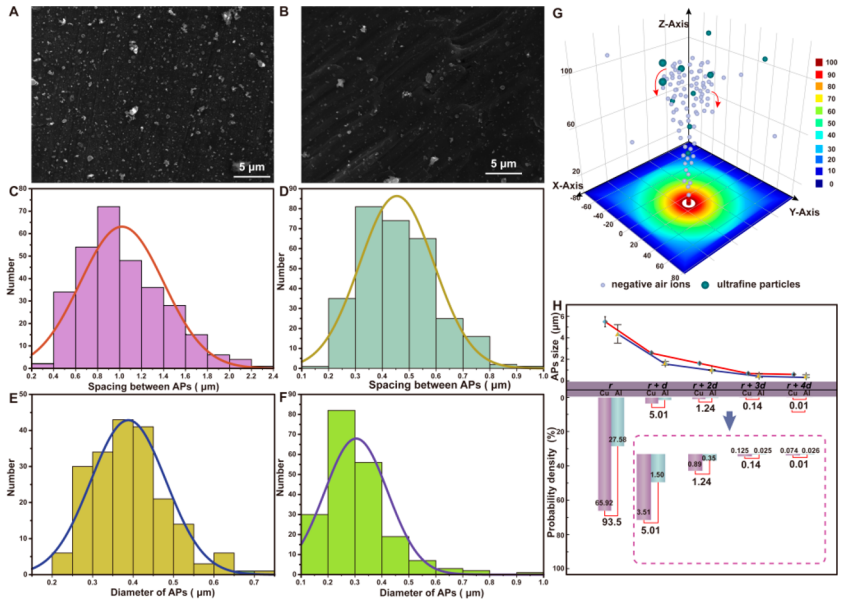

Figure 1. Information about APs on copper wires and aluminum wires. SEM images of APs adsorbed on copper wire (A) and aluminum wire (B); spacing distance distribution between adjacent APs on copper wire (C) and aluminum wire (D); particle size distributions of APs on copper wire (E) and aluminum wire (F). Schematic diagram of NAIs trajectory simulation (G) and probability density of FPs absorbed on different conductors (H).

microscopic structure information about the collected APs was derived from high-resolution scanning electron microscopy (SEM). The detailed numerical information, including the size, quantity, and distribution of APs, was obtained by analyzing more than 300 SEM pictures. A conductive sponge is a good electromagnetic shielding material. According to the obtained migration and distribution trends of fine particles under the influence of NAIs, we applied a nickel coated polyester sponge to replace the indoor adsorption interface for collecting the SAPs. The results show that it can effectively alleviate the SAPs caused by NAIs.

EXPERIMENTAL SECTION

Materials and Chemicals. Copper wire, aluminum wire, and iron wire were purchase from a local retail store. ITO glass ($10 \times 10 \times 1.1$ mm^3, ≤ 8 Ω/sq) was obtained from Beijing Hualid Technology Co., Ltd., China. Carbon double-sided tape was purchased from Nisshin EM Co., Ltd., Japan. A polyester sponge with foaming pore size of 0.3 mm was purchased from Shenzhen Huayueyuan Electronics Co., Ltd., China.

Collection of Specific Aggregated Particles. All samples were collected in laboratory conditions, in Beijing. To facilitate sample preparation, we set up a set of devices on the wall to simulate the formation process of SAPs, as shown in Figure S1. Different materials were fixed on the wall to collect APs. The gas coming out of the vent is supplied by an air pump with a gas flow meter, and the gas flow rate is consistent with that of the normal air purification system, about 5 L^3/s. The collection time for all samples is 90 h, which is equivalent to the total amount of mobile charge generated by the air purification system with negative air ions mode in one season. In order to ensure the accuracy of the experimental results, we did not collect samples in specific weather, such as rain and haze, and 38 samples were collected during the entire experiment.

Characterization of Collected Particles. In order to characterize the collected particles, four factors need to be analyzed, namely, the microscopic morphology, quantity, dynamic diameter, and element composition of the particles.

Microscopic Morphology. The morphological characterization of all samples was achieved by ultrahigh resolution scanning electron microscopy (Sirion 200, Holland). The aggregated particles were collected directly on different conductive wires or other materials, as shown in Figure S1. The scanning voltage was 15.00 kV in ultrahigh-resolution mode, and at least five sites were selected for each sample.

Quantity and Size. The amount and size of the APs were measured by using Nano Measurer 1.2 software. According to the SEM results, we randomly selected at least 200 particles for measuring the average sizes of APs. Specific statistical methods are described as follows: Randomly select the same area (20×20 μm) in SEM images and then measure the particles in the area (note: some interference impurities, such as fibers, pollutants on adsorption carriers should be excluded). When measuring the distance between two adjacent particles, it is necessary to select the nearest particle and measure its linear distance. Meanwhile, we assume that the particle is a regular sphere, and take its plane diameter as the results.

Elemental analysis. We collected four samples for elemental analysis at room temperature. The aggregation time of these four samples is identical but under different conditions, ensuring the total amount of elements. The elemental analysis was performed by X-ray photoelectron spectroscopy (XPS, PHI QUANTRO SXM, ULVAC-PHI, Japan). Specific parameters are as follows: hemispherical energy analyzer, monochromatic Al target, X-ray beam spot 100 μm, incident angle 45°, analysis chamber vacuum is better than 1.0×10^{-7} Torr. Full spectrum: pass energy 280 eV, step length 1.0 eV; narrow spectrum: pass energy 55 eV, step length 0.1 eV. The details of the element composition are listed in Table S1.

https://doi.org/10.1021/acsomega.2c00290
ACS Omega 2022, 7, 11285−11292

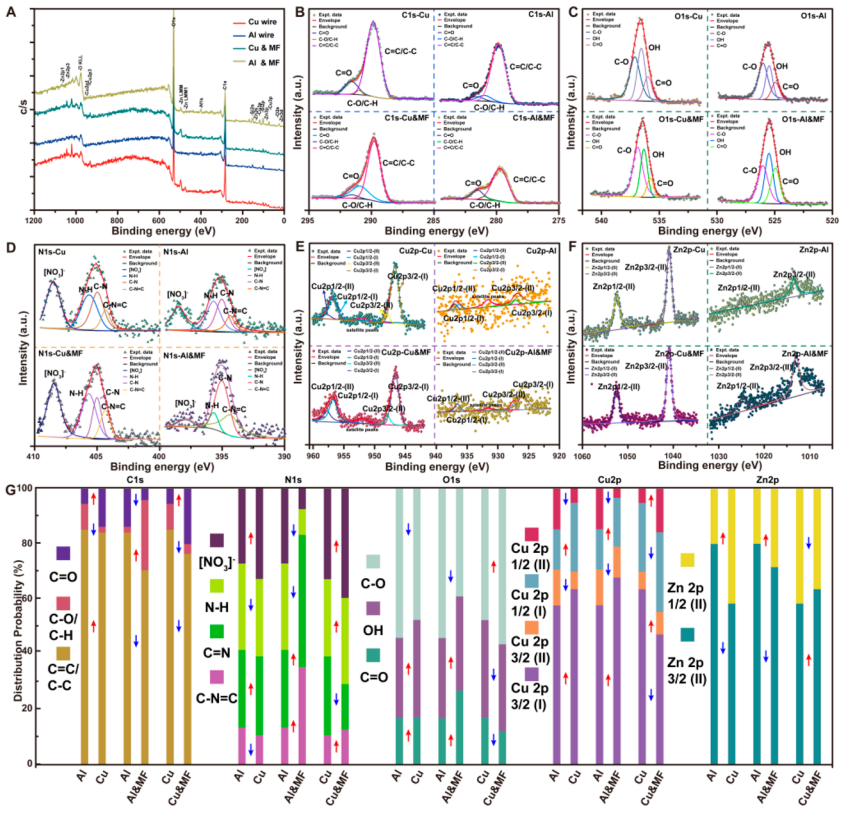

Figure 2. XPS spectra of APs collected from different conditions, including four samples on copper wire and aluminum wire with or without a magnetic field. Wide scan spectra (A); high-resolution spectra of C 1s, O 1s, N 1s, Cu 2p, and Zn 2p (B−F); relative content and tendency of characteristic functional groups under different conditions (G).

Preparation of Nickel Coated Polyester Sponge. The sponge was cut into stripes of 5 mm × 3 mm × 2 m . The stripe were put into a vertical oven to dry for 24 h at 90 °C. Then, the sponge stripe was evenly pasted onto one side of the carbon double-sided tape and pressed for 1 h. Finally, the dried sponge was put into the magnetron sputtering coating machine for vacuum nickel coating. Parameter conditions: prepumped background pressure 1.0×10^{-2} Pa, working pressure 1.2×10^{-1} Pa, flow rate of argon gas 120 sccm, pressure of argon gas 0.1 M Pa, planar rectangular single target sputtering power 5 kW, operating line speed 0.5 m/min, nickel target purity >99.95%.

RESULTS AND DISCUSSION

Negative air ions can cause specific aggregation of suspended particles on the surface of indoor objects. We firmly believed that an extremely complex physical and chemical reaction occurred during the aggregation progress. The evidence supporting our viewpoint can be summarized as follows: (i) the aggregated particles are not adsorbed on the wall uniformly but in a specific location without any external turbulence flows, and over time the walls turn black; (ii) it is extremely difficult to clean up because the microstructure of the APs is particularly compact; (iii) the chemical properties, including the oxidation−reduction property, stability, and compositions, have changed dramatically. In order to better comprehend the essence of SAPs, it is necessary to elaborate the formation process and its main influencing factors.

Conducting Capability of the Adsorption Surface Determines the Migration Direction of Fine Particles. We simulated the formation of SAPs in the laboratory to reveal the mechanism of the negative air ions causing the specific aggregation of fine particles. The experimental device used for collecting APs as shown in Figure S1. The copper wires and aluminum wires were fixed on the wall. The parameters of these two wires are listed in Table S2. All conductive wires are connected to zero potential in order to avoid the influence of electric field deviation, so there is no obvious difference of potential between the wires and the wall.

Figure 1 illustrates the information for APs adsorbed on conductive wires. As shown in Figure 1A and B, the density of APs on copper wire is much higher than that of aluminum wire. The physical parameters of these two wires are almost identical, including the diameter, length, and potential, except for conductivity. We analyzed the parameters of APs, including the density, diameter, and distribution probability on different adsorption carriers. In Figure 1C and D, the spacing distribution of adjacent APs on copper wire and aluminum wire is mainly located in the ranges of 0.1−1.0 and 0.2−2.4 μm, respectively. More than 73% of the APs on copper wire are in the range of 0.35−0.55 μm; however, the spacing distance between adjacent APs on the aluminum wire is approximately 58% distributed in the range of 0.7−1.1 μm. The results indicate that the density of APs on copper wire is much higher than that on aluminum wire. In addition, we also randomly measured the diameter size of 200 APs on both wires. Figure 1E and F exhibits the diameter size of APs adsorbed on copper wire and aluminum wire, respectively. APs on copper wire are mainly between 0.25 and 0.45 μm, with an average size of about 0.39 μm. However, the APs on aluminum wire ranged from 0.15 to 0.35 μm, with an average size of nearly 0.30 μm.

https://doi.org/10.1021/acsomega.2c00290
ACS Omega 2022, 7, 11285−11292

Assuming the single fine particle as a homogeneous sphere, the average diameter is approximately 87.7 nm according to the results in Figure S2. A single APs on copper wire was made up of 87.94 FPs, while on aluminum wires it was made up of about 40.03 FPs. The amount of FPs adsorbed on the copper wire is more than 2 times that on the aluminum wire. However, this is only the disparity of one single AP. When the total amount of APs in the same region ($20 \times 20\ \mu m^2$) is considered, the gap widens further. In Figure 1H, the FPs adsorbed at different locations have an obvious difference. We simulated the falling point distribution tendency of free charges of about 89.7% FPs adsorbed on copper wire, while just 10.2% FPs adsorbed on aluminum wire; moreover, only 0.1% adsorbed on the wall surface, as shown in Figures 1G and S4. NAIs tend to move toward the place where there is good conductivity capacity. Millions of NAIs spew out from the tip of the carbon electrode to form a relatively stable high energy potential field, as shown in Figure S3. The final moving velocity of FPs in this field is related to the electric field strength and diameter of the particles, which is positively correlated with electric field strength and negatively correlated to particle size. In other words, multiple free charges can propel smaller particles to move quickly.

NAIs produced by the corona discharge would be carried by airflow to a space far from the wall, forming a relatively high energy field in the *x*-axis direction. Free charges in high-energy fields tend to move toward a lower energy field to maintain equilibrium. There are two ways to maintain equilibrium: one is charge quenching, and the other one is conducting the charges away through conductors. A nonuniform electric field exists between the high energy field and the wall surface, so that the free charges will move toward the direction of the lower electric field. The high-energy charges are more easily conducted by wires with high conductivity when the free charges are in contact with the wall and conductive wires. Although the area of wall surface exposure to NAIs is much larger than that of conductive wires, the FPs adsorbed on the surface of the wall, copper wire, and aluminum wire have an obvious difference. The number of APs is consistent with the strength of the electrical conductivity. This means that free charges are more inclined to migrate to the position with good conductivity, resulting in a significant increase in the density of APs. This is enough to show motion behavior of FPs, especially that the motion direction is indeed affected by NAIs.

Surface Reaction Affects the Stability of Aggregated Particles. It is difficult to use common physical methods, including sandpaper grinding and solvent dissolution, to remove the SAPs completely. Hence, the physical and chemical properties of APs formed by FPs have changed significantly. The chemical elemental composition of APs was characterized by X-ray spectroscopy, and the element contents on surface are listed in Table S1. The main peaks in Figure 2A represent the signals of C 1s, N 1s, O 1s, Si 2p, Cu 2p, and Zn 2p. The common elements in all cases are C 1s, N 1s, O 1s, and Si 2p, in which the surrounding binding energy is 284.8, 400.5, 531.5, and 102.3 eV, respectively. Two obvious conclusions can be drawn from the XPS spectrum. First, the changes in the valence states of elements, the relatively stable valence states, increased significantly. Second, element content increased, such as Cu and Zn in Figure 2E and F.

According to Figure 2B, the high-resolution spectra of C 1s is mainly composed of C═C/C−C, C−O/C−H, C═O, corresponding to the binding energies of 284.6, 286.8, and 288.1 eV, respectively. The secondary content element is O 1s. From Figure 2C, O 1s binds with carbon and hydrogen in C═O (530.5 eV), OH (531.68 eV) and C−O (532.81 eV), in which C−O is the dominant state. In Figure 2D, C−N═C, C−N, N−H, NO_3^- are the four chemical bonds, corresponding to the peaks at 398.67, 400.0, 401.37, and 407.05 eV, in which NO_3^- has the maximum abundance. As the most important characteristic functional group of nitrates, we speculate that the nitrogen element mainly exists in the form of nitrate in APs. Figure 2E and F displays the metal elements detected in all cases. The Cu 2p peaks at 932.66 and 952.5 eV correspond to Cu 2p3/2 and Cu 2p1/2, respectively, representing the state of Cu^+ in APs; moreover, the peaks of 935.14 and 954.5 eV correspond to Cu 2p3/2 and Cu 2p1/2 of Cu^{2+}, respectively. This means that Cu 2p mainly exists in the form of Cu^+ and Cu^{2+} ions in solid particles. In addition, Zn 2p consists of the form of Zn^{2+}, corresponding to the peaks at 1021.2 and 1044.8 eV for Zn 2p3/2 and Zn 2p1/2, respectively. These results from XPS can only demonstrate the existence of elements in APs. Further analysis is needed to explore the trend of corresponding content variation under different conditions.

In our previous work, we mainly analyzed the effect of NAIs on specific organic compounds in particulate matter.[20] However, we consider it more important to summarize the commonalities of compounds in APs. Therefore, we want to know more about the mechanism of the physical-chemical reaction between particles and NAIs through the structural changes in the composition of the compounds. As shown in Figure S5, we set two repulsive neodymium magnets beside the conductive wires. The magnetic field (MF) strength at the site of these two wires is about 87 mT. When the moving charge vertically into the MF, it will deflect and eventually adsorb on the wires. We set three control groups: the first one is APs collected from aluminum wire and copper wire without MF; the second group is APs collected from copper wire without MF and with MF; the third group is samples collected from aluminum wire without MF and with MF. The commonality of these groups is that the conductivity of the latter one is higher than that of the former, which can lead to the increase of electron flux.

The changes of chemical states are summarized in Figure 2G. Changes in the second group and third group were compared based on the first group. The relatively stable valence state, especially the content of oxygen-containing groups, increases significantly with the increase of NAIs. This is consistent with our conclusion that the free charges can effectively change the physical and chemical properties of APs, especially to improve its stability. In the first and third groups, the relative content of the most stable state of C═O improved more than two times. The C═C and C−H content decreased most obviously due to the oxidizing effect. However, C═O decreased due to the preferential consumption of reactive oxygen by aluminum wires in the second group. In order to verify our inference, the changes in the oxygen state were analyzed. Oxygen mainly exists in three oxygen-containing functional groups, such as C−O, O−H, and C═O. The total content of oxygen in APs was listed in Table S1. We found that when the content of reactive oxygen is constant, unstable functional groups will turn to more stable ones under the influence of NAIs. This may be attributed to that when reactive oxygen participates in the reaction, it is more likely to form functional groups such as C−O and O−H with weaker bond

https://doi.org/10.1021/acsomega.2c00290
ACS Omega 2022, 7, 11285−11292

energy and will shift to steady-state due to the action of NAIs, which means NAIs not only can cause changes in the content of oxygen, but also can affect the stability of oxygen-containing materials in APs.

The nitrogen element has no obvious regularity for two reasons. One is that nitrogen exists in both inorganic nitrates and nitrogenous organics, which have different responses to the external environment. The results showed that the relative content of nitrate had nearly no change under normal conditions. The nitrogen-containing functional groups are significantly affected by the outside environment, especially oxides. Second, the analysis of specific nitrogen-containing functional groups is not persuasive because the total amount of nitrogen in organic compounds is lower. The relative contents of N−H, C−N and C−N═C are in the ranges of 0.24−1.01, 0.52−1.26 and 0.27−0.93%, respectively. However, the overall regularity in nitrogenous organic compounds is basically the same as that of carbon and oxygen; that is, the NAIs can effectively change the state of the nitrogenous substance. The relatively unstable valence states will change to stable states under the action of NAIs. The characteristic functional groups, especially C═N and N−H, are more remarkable.

Subsequently, the metal elements show good consistency with our estimation, too. The positions of the Cu 2p3/2-(I), Cu 2p1/2-(II), Zn 2p3/2-(II), and Zn 2p1/2-(II) peaks in all samples are almost identical, indicating these two elements have the same oxidation state. In all control groups, the content of metal elements increased significantly especially under conditions of increased electron flux. This may be because metal elements are more sensitive to magnetic fields. Therefore, we speculate that substances with strong oxidizing properties have participated in the reaction.[21] Strong oxidizing ions in NAIs can oxidize unsaturated bonds on the surface of FPs rapidly, especially the small molecule VOCs. Most of the metal elements in APs exist in a more stable state rather than in a high oxidative state and the magnitude of the change is not obvious, due to the metal elements mostly existing in the form of oxides, such as Cu_2O, CuO, and ZnO, in which their reducibility is less than that of unsaturated organic matter. Therefore, NAIs initiated the surface reaction of FPs and changed the stability of FPs.

Surface Roughness Determines the Final Amount of Aggregated Fine Particles. The final location site and the amount of APs are related to the characteristics of the adsorption interface. To illustrate the adsorption mechanism, we fixed four different materials on the wall (ITO glass, iron wire, aluminum wire, and copper wire) and placed them in the same environment (zero potential and same concentration of NAIs). The terminal morphology of APs adsorbed on these four materials is shown in Figure 3. After 60 h of enrichment, few APs adsorbed on ITO glass (Figure 3A), and the amount of APs on iron wire (Figure 3B) was also less than that for aluminum wire (Figure 3C) and copper wire (Figure 3D). In addition to the influence of conductivity, the amount of APs depends on the roughness of the adsorption interface. A linear simulation curve was drawn based on surface roughness information and particle size for these four materials, as shown in Figure 3E.

We suggest that the adsorption and aggregation processes of fine particles at the interface and the eventual formation of SAPs are as follows: Fine particles surrounded by NAIs tend to migrate to the position with weak potential. Due to its own potential energy, electrical energy is released when in contact

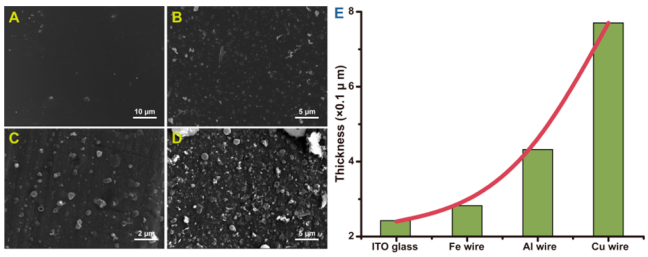

Figure 3. SEM images of APs adsorbed on materials with different roughness (A−D) and the tendency relationships between adsorption amount and material roughness (E).

with the adsorption surface. There are many small bumps in the microstructure of the rough and uneven adsorption surfaces, which are similar to lightning rods. When charged particles encounter these small bumps or other substances on the interface, their potential energy will be transmitted and deposited near the small bumps and they finally form small APs. Then, these small APs play as the role of nucleus to adsorb other particles and eventually form larger APs. The process is roughly shown in Figure S6. In addition, these charged particles will hit the adsorption surface at a fast speed by the acceleration effect of the electric field, and the uneven structure is more conducive to the location of particles. This may be the reason why the SAPs have such a compact structure and why they often appear around rough interfaces rather than smooth interfaces, such as glass, marble, etc.

Nickel Coated Conductive Sponge Used for Delaying the Adsorption of Fine Particles on the Indoor Surface. According to the above information, we knew clearly about the distribution regularity of indoor FPs influenced by NAIs. We proposed a porous conductive sponge with high specific surface area and high conductivity as the adsorption interface for indoor suspended particles. The fabrication process of the nickel coated conductive sponge (NCCS) is illustrated in Figure 4A. In this section, a thin Ni film was deposited on the polyester sponge via vacuum coating technology. The explanation for using the nickel coating is that, first, it is cost effective; second, the operating conditions are relatively mild when compared with other conductive metals, and its electrical conductivity can fully meet the needs of this work; third, nickel is one of the most widely used metals in electromagnetic shielding fields, so it may be more convenient for the popularization and application of this method. The characterization of the SEM-EDS spectrum of the prepared sponge is shown in Figure 4B, which indicates that the nickel has been successfully coated onto the sponge. Next, we fixed NCCS on the indoor wall surface, which was around the NAIs generator or the high energy field formed by NAIs in the x-axis direction, as shown in Figure 4C.

We carefully compared the APs on NCCS and ITO glass under the same concentration of NAIs. Figure 5A shows the APs on NCCS, in which we can find that the NCCS has an obvious adsorption effect on FPs affected by NAIs. Fine particles surrounded by NAIs will adsorb on the Ni film due to electrostatic migration. The electrostatic charge experiment was performed to verify this point, as shown in Figure S7. The amount of electrostatic charge has changed significantly before and after the adsorption of APs, which means this material can transfer the free charges of NAIs effectively. Particles will continuously aggregate on the Ni surface to form APs of different size. Meanwhile, we compared the APs on the ITO

https://doi.org/10.1021/acsomega.2c00290
ACS Omega 2022, 7, 11285−11292

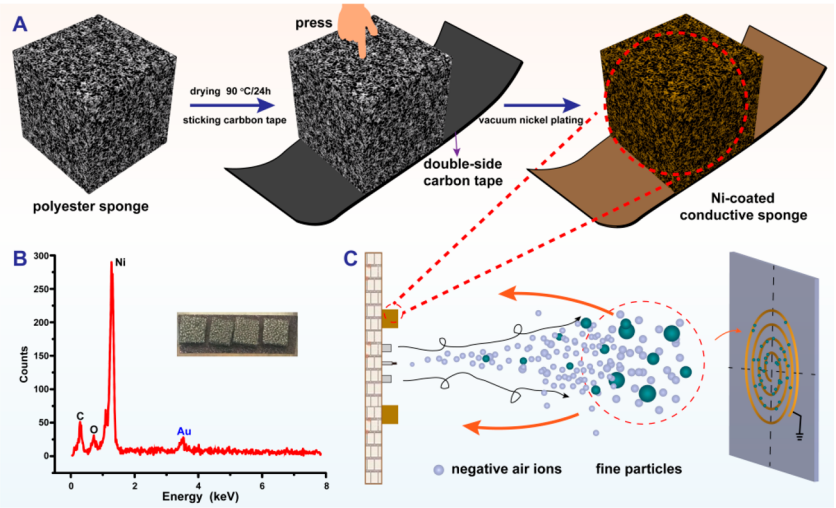

Figure 4. Schematic of preparation steps of NCCS (A). Spectra of the SEM-EDS analysis for the prepared sponge (B). Application of the NCCS for capture the suspended fine particles affected by NAIs (C).

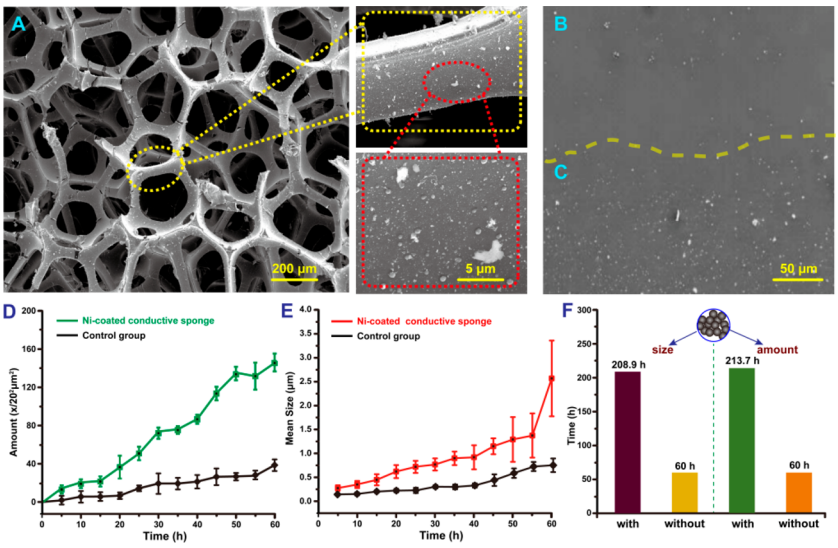

Figure 5. Effect of NCCS on FPs. SEM images of APs on NCCS (A); comparison of particles adsorbed on the same adsorption interface with and without the sponge (B,C); amount and size of APs adsorbed on NCCS and ITO glass (D,E); time comparison of FPs reaching the same size and quantity with or without NCCS (F).

glass surface under the conditions with and without NCCS as shown in Figure 5B and C, respectively. We found that the FPs were mainly adsorbed on the surface of nickel film in the presence of NCCS and only a few particles fell on the ITO glass. However, the particles on the ITO glass increased significantly when there was no NCCS. Changes in the number and size of APs on NCCS and ITO glass during different periods are shown in Figure 5D and E. After 60 h, the average amounts of APs on NCCS and ITO are approximately 146.23 and 41.05, respectively; in addition, the average diameter of the APs is about 2.58 and 0.74 μm, respectively. Based on the average number and average size of the APs at 60 h, we roughly estimated the time for the particles to reach the above-mentioned level on the normal surface with NCCS, as shown in Figure 5F. The results show that it takes 213.7 and 208.9 h, respectively. This means that NCCS is a good adsorption material for capturing APs and can effectively delay the specific adsorption of FPs affected by NAIs on the indoor surface. We also evaluated the durability of NCCS, and its service life is positively correlated with the total amount of the fixed NCCS, especially the total specific surface area.

CONCLUSIONS

In summary, the anomalous aggregation of fine particles caused by negative air ions is different from either gravitational settling or turbulent layer deposition. Directional migration and fixed-point enrichment are characteristics of this aggregation mode. The existence of NAIs is the basic prerequisite of specific aggregated particles. NAIs will migrate to the position with low potential, causing the comigration of suspended fine particles. Strong oxidizing ions in NAIs can further oxidize the components on the surface of particles to form stable compounds. The conductivity and roughness of the adsorption interface are the physical factors affecting the formation of SAPs. Under same potential energy, the NAIs are often adsorbed on the surface with strong electrical conductivity. The microconvex structure of the adsorption interface will be

https://doi.org/10.1021/acsomega.2c00290
ACS Omega 2022, 7, 11285−11292

used as growth core and further enriched to form larger particles.

The nickel coated polyester sponge can be used as a good material to solve the problem of indoor fine particle specific aggregation caused by negative air ions. This conductive sponge with high conductivity and high specific surface area can effectively delay the aggregation of fine particles on the surfaces of indoor objects. Before the interface reaches saturation, the fine particles will preferentially accumulate on the conductive sponge. According to the experimental results, the adsorption of particles on other interfaces can be effectively delayed by more than 3 times and this delay efficiency is related to the amount of conductive sponge used.

■ ASSOCIATED CONTENT

Supporting Information

The Supporting Information is available free of charge at https://pubs.acs.org/doi/10.1021/acsomega.2c00290.

> Calculation method for APs in a square area; information on atomic concentration, adsorption materials, and proportion of functional groups; experimental devices, SEM characterization spectra, supplemental notes, and electrostatic charge experiment (PDF)

■ AUTHOR INFORMATION

Corresponding Authors

Jin-Ming Lin − *Department of Chemistry, Beijing Key Laboratory of Microanalytical Methods and Instrumentation, Tsinghua University, Beijing 100084, PR China;* orcid.org/0000-0001-8891-0655; Email: jmlin@mail.tsinghua.edu.cn

Zenghe Li − *School of Chemistry, Beijing University of Chemical Technology, Beijing 100084, PR China;* Email: lizh@mail.buct.edu.cn

Authors

Chaoying Zhang − *Department of Chemistry, Beijing Key Laboratory of Microanalytical Methods and Instrumentation, Tsinghua University, Beijing 100084, PR China; School of Chemistry, Beijing University of Chemical Technology, Beijing 100084, PR China;* orcid.org/0000-0002-5709-7152

Zengnan Wu − *Department of Chemistry, Beijing Key Laboratory of Microanalytical Methods and Instrumentation, Tsinghua University, Beijing 100084, PR China;* orcid.org/0000-0002-3766-2994

Haifeng Lin − *Department of Chemistry, Beijing Key Laboratory of Microanalytical Methods and Instrumentation, Tsinghua University, Beijing 100084, PR China*

Complete contact information is available at: https://pubs.acs.org/10.1021/acsomega.2c00290

Author Contributions

This manuscript was supported by all authors. All authors have approved the final version of the manuscript.

Funding

The National Natural Science Foundation of China (21621003) is acknowledged for financial support.

Notes

The authors declare no competing financial interest.

■ ACKNOWLEDGMENTS

The authors would like to thank Dr. Xinchang Gao for his assistance with XPS characterization.

■ REFERENCES

(1) Lee, C. J.; Martin, R. V.; Henze, D. K.; Brauer, M.; Cohen, A.; Donkelaar, A. v. Response of global particulate-matter-related mortality to changes in local precursor emissions. *Environ. Sci. Technol.* **2015**, *49* (7), 4335−4344.

(2) Lim, S. S.; Vos, T.; Flaxman, A. D.; Danaei, G.; Shibuya, K.; Adair-Rohani, H.; AlMazroa, M. A.; Amann, M.; Anderson, H. R.; Andrews, K. G.; et al. A comparative risk assessment of burden of disease and injury attributable to 67 risk factors and risk factor clusters in 21 regions, 1990−2010: a systematic analysis for the Global Burden of Disease Study 2010. *Lancet* **2012**, *380* (9859), 2224−2260.

(3) Franchini, M.; Mannucci, P. M. Thrombogenicity and cardiovascular effects of ambient air pollution. *Blood, J. Am. Soc. Brew. Chem. Hema* **2011**, *118* (9), 2405−2412.

(4) Ohlwein, S.; Kappeler, R.; Joss, M. K.; Künzli, N.; Hoffmann, B. Health effects of ultrafine particles: a systematic literature review update of epidemiological evidence. *Int. J. Public Health* **2019**, *64* (4), 547−559.

(5) Von Schneidemesser, E.; Monks, P. S.; Allan, J. D.; Bruhwiler, L.; Forster, P.; Fowler, D.; Lauer, A.; Morgan, W. T.; Paasonen, P.; Righi, M.; et al. Chemistry and the linkages between air quality and climate change. *Chem. Rev.* **2015**, *115* (10), 3856−3897.

(6) Tan, J.; Duan, J.; Zhen, N.; He, K.; Hao, J. Chemical characteristics and source of size-fractionated atmospheric particle in haze episode in Beijing. *Atmos. Res.* **2016**, *167*, 24−33.

(7) Mellouki, A.; Wallington, T.; Chen, J. Atmospheric chemistry of oxygenated volatile organic compounds: impacts on air quality and climate. *Chem. Rev.* **2015**, *115* (10), 3984−4014.

(8) Zhang, R.; Wang, G.; Guo, S.; Zamora, M. L.; Ying, Q.; Lin, Y.; Wang, W.; Hu, M.; Wang, Y. Formation of urban fine particulate matter. *Chem. Rev.* **2015**, *115* (10), 3803−3855.

(9) Gupta, A.; Bhandari, M. Monitoring and control of particulate matter in indoor air: a review. *J. Appl. Nat. Sci.* **2011**, *3* (1), 139−150.

(10) Zhao, X.; Li, Y.; Hua, T.; Jiang, P.; Yin, X.; Yu, J.; Ding, B. Low-resistance dual-purpose air filter releasing negative ions and effectively capturing $PM_{2.5}$. *ACS Appl. Mater. Interfaces* **2017**, *9* (13), 12054−12063.

(11) Wang, C.-S.; Otani, Y. Removal of nanoparticles from gas streams by fibrous filters: a review. *Ind. Eng. Chem. Res.* **2013**, *52* (1), 5−17.

(12) Zhang, C.; Wu, Z.; Wang, C.; Li, H.; Li, Z.; Lin, J.-M. Hydrated negative air ions generated by air−water collision with TiO_2 photocatalytic materials. *RSC Adv.* **2020**, *10* (71), 43420−43424.

(13) Zhang, S.; Liu, H.; Yin, X.; Yu, J.; Ding, B. Anti-deformed polyacrylonitrile/polysulfone composite membrane with binary structures for effective air filtration. *ACS Appl. Mater. Interfaces* **2016**, *8* (12), 8086−8095.

(14) Wang, S.; Zhao, X.; Yin, X.; Yu, J.; Ding, B. Electret polyvinylidene fluoride nanofibers hybridized by polytetrafluoroethylene nanoparticles for high-efficiency air filtration. *ACS Appl. Mater. Interfaces* **2016**, *8* (36), 23985−23994.

(15) Jaworek, A.; Marchewicz, A.; Sobczyk, A.; Krupa, A.; Czech, T. Two-stage electrostatic precipitators for the reduction of $PM_{2.5}$ particle emission. *Prog. Energy Combust. Sci.* **2018**, *67*, 206−233.

(16) Yu, K.-P.; Lee, G. W.-M.; Lin, S.-Y.; Huang, C. P. Removal of bioaerosols by the combination of a photocatalytic filter and negative air ions. *J. Aerosol Sci.* **2008**, *39* (5), 377−392.

(17) Sawant, V.; Meena, G.; Jadhav, D. Effect of negative air ions on fog and smoke. *Aerosol Air Qual. Res.* **2012**, *12* (5), 1007−1015.

(18) Liu, W.; Huang, J.; Lin, Y.; Cai, C.; Zhao, Y.; Teng, Y.; Mo, J.; Xue, L.; Liu, L.; Xu, W.; et al. Negative ions offset cardiorespiratory benefits of $PM_{2.5}$ reduction from residential use of negative ion air purifiers. *Indoor air* **2021**, *31* (1), 220−228.

(19) Salthammer, T.; Fauck, C.; Schripp, T.; Meinlschmidt, P.; Willenborg, S.; Moriske, H.-J. Effect of particle concentration and semi-volatile organic compounds on the phenomenon of 'black magic dust' in dwellings. *Build. Environ* **2011**, *46* (10), 1880−1890.
(20) Zhang, C.; Wu, Z.; Li, Z.; Li, H.; Lin, J.-M. Inhibition effect of negative air ions on adsorption between volatile organic compounds and environmental particulate matter. *Langmuir* **2020**, *36* (18), 5078−5083.
(21) Duncan, S.; Sexton, K. G.; Turpin, B. Oxygenated VOCs, aqueous chemistry, and potential impacts on residential indoor air composition. *Indoor Air* **2018**, *28* (1), 198−212.

https://doi.org/10.1021/acsomega.2c00290
ACS Omega 2022, 7, 11285−11292